Simulation of Moving-bed and Fluidized-bed Reactors by DPM and MPPIC in OpenFOAM

The 11th OpenFOAM® Workshop

26-30 June 2016
Vila Flor Cultural Centre, Guimarães, Portugal

Kwonwoo Jang, Woojoo Han, Kang Y. Huh
Pohang University of Science and Technology

POSTECH
Combustion Laboratory

Contents

1. Introduction

2. Physical Models

3. Code Development

4. Applications

5. Summary

Introduction

Metallurgical Processes

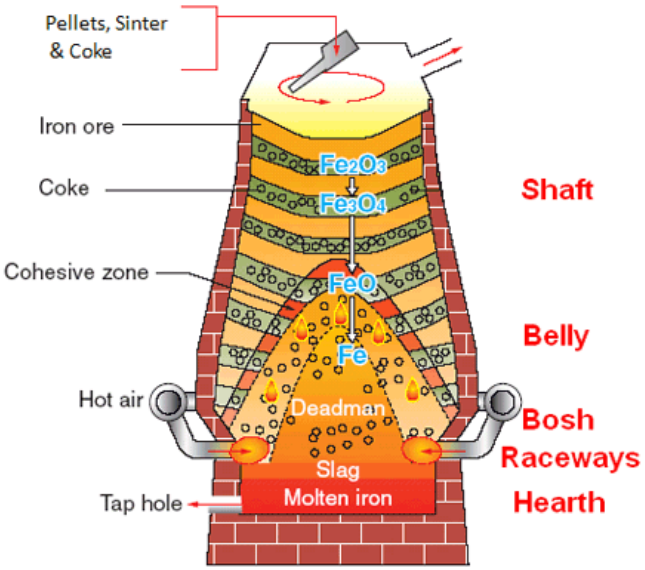

Blast Furnace

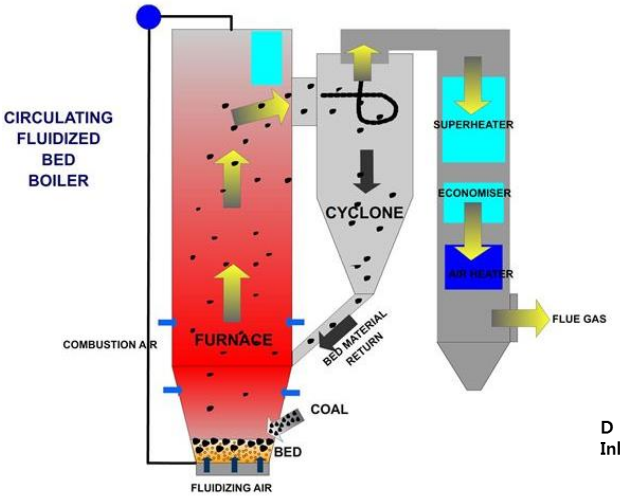

Circulating Fluidized Bed

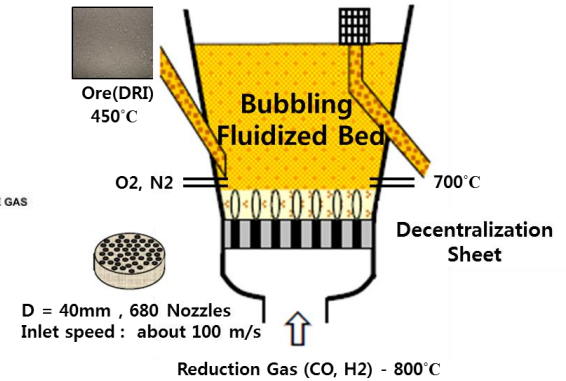

Bubbling Fluidized Bed

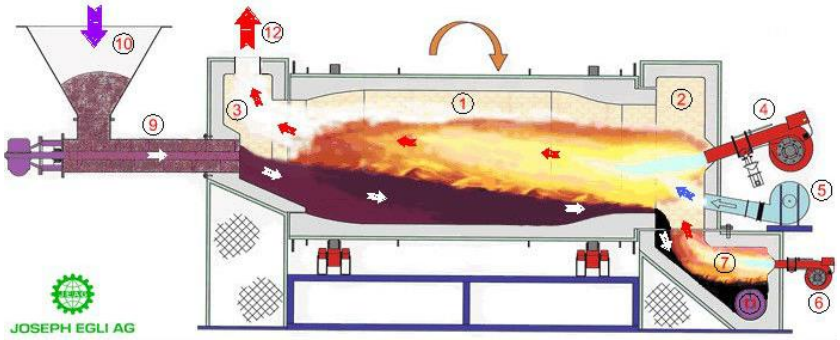

Rotary Klin

- Contains high particle concentrations involving chemical reaction.
- Widely used in steel making processes, energy conversion, etc.
- Development of relevant submodels in OpenFOAM.

Introduction

Physics

Particle Motion

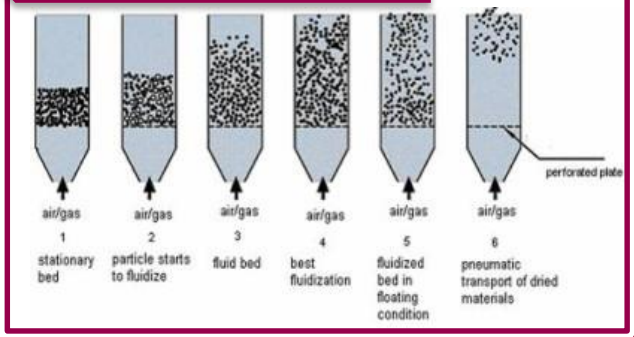

Heat Transfer

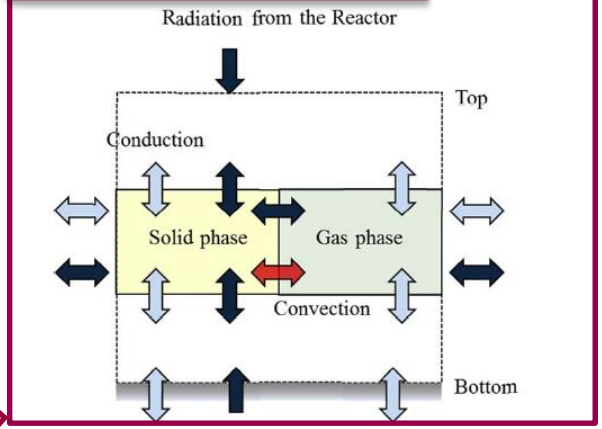

Metallurgical Process

Heterogeneous Reaction

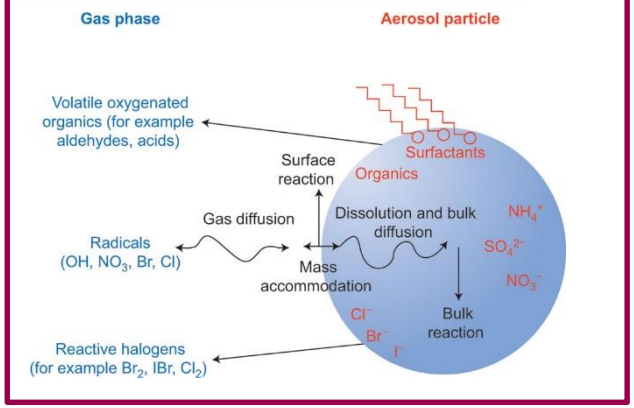

Turbulent Combustion

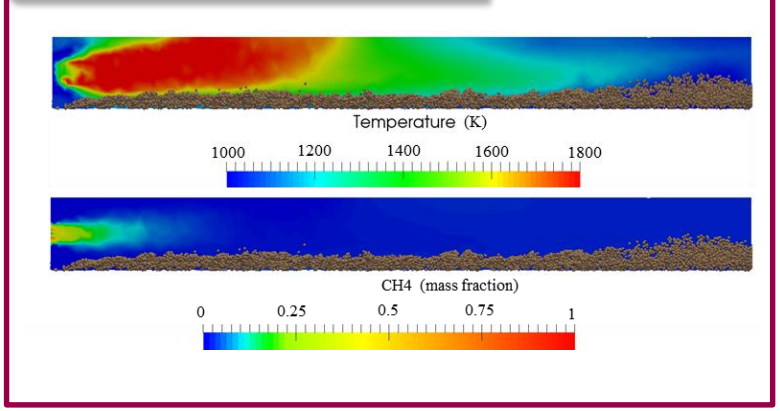

Physical Models - Eulerian vs Lagrangian

Computational Approaches for Particle Motion

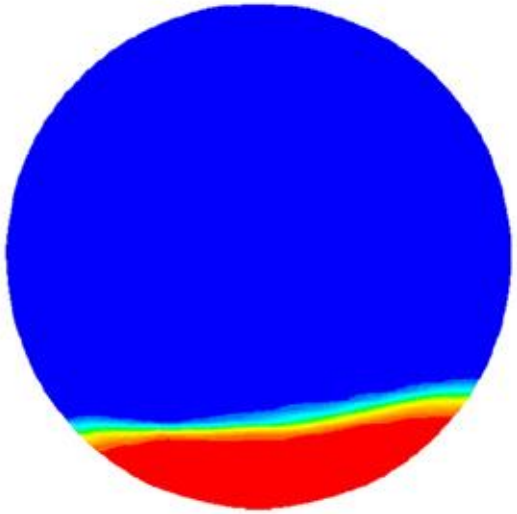

Eulerian - Eulerian

Eulerian - Lagrangian

- Eulerian : Particle bed assumed in another fluid phase
  - Advantage : Low computational cost
  - Disadvantage : Inter-particle or particle-gas Interaction described by empirical formulae.
- Lagrangian : Tracking each particle or parcel motion independently
  - Advantage : Consider impact stress and micro scale motion of particles
  - Disadvantage : High computation cost

Physical Models - Eulerian-Eulerian

Eulerian-Eulerian Approach [1]

Multiphase CFD

Eulerian-Eulerian

$$\frac{\partial(\theta_f \rho_f)}{\partial t} + \nabla \cdot (\theta_f \rho_f \mathbf{u}_f) = 0$$

$$\frac{\partial(\theta_s \rho_s)}{\partial t} + \nabla \cdot (\theta_s \rho_s \mathbf{u}_s) = 0$$

Two Fluid Model

$$\frac{\partial(\theta_f \rho_f \mathbf{u}_f)}{\partial t} + \nabla \cdot (\theta_f \rho_f \mathbf{u}_f \mathbf{u}_f) = -\theta_f \nabla P + \nabla \cdot \boldsymbol{\tau} + \theta_f \rho_f \mathbf{g} + K_{gs}(\mathbf{u}_s - \mathbf{u}_f)$$

$$\boldsymbol{\tau} = \theta_f \mu_f (\nabla \mathbf{u}_f + (\nabla \mathbf{u}_f)^T) - \frac{2}{3}\theta_f \mu_f (\nabla \cdot \mathbf{u}_f)\boldsymbol{\delta}$$

Granular temperature equation

$$\frac{3}{2}\left[\frac{\partial(\theta_s \rho_s G_s)}{\partial t} + \nabla \cdot (\theta_s \rho_s G_s \mathbf{u}_s)\right] = (-P_s \mathbf{I} + \boldsymbol{\tau}_s) : \nabla \mathbf{u}_s + \nabla \cdot (k_{G_s} \nabla G_s) - \gamma_{G_s} + \varphi_{gs}$$

$$P_s = \theta_s \rho_s G_s + 2\rho_s (1+e_{ss})\theta_s^2 g_{0,ss} G_s$$

$$\mu_s = \frac{4}{5}\theta_s^2 \rho_s d_s g_{0,ss}(1+e_{ss})\left(\frac{G_s}{\pi}\right)^{1/2} + \frac{\theta_s d_s \rho_s \sqrt{G_s \pi}}{6(3-e_{ss})}\left[1 + \frac{2}{5}(1+e_{ss})(3e_{ss}-1)\theta_s g_{0,ss}\right]$$

$$\lambda_s = \frac{4}{3}\theta_s \rho_s d_s g_{0,ss}(1+e_{ss})\left(\frac{G_s}{\pi}\right)^{1/2}$$

$$g_{0,ss} = \left[1 - \left(\frac{\theta_s}{\theta_{s,\max}}\right)^{1/3}\right]^{-1}$$

$$\frac{\partial(\theta_s \rho_s \mathbf{u}_s)}{\partial t} + \nabla \cdot (\theta_s \rho_s \mathbf{u}_s \mathbf{u}_s) = -\theta_s \nabla P + \nabla P_s + \nabla \cdot \boldsymbol{\tau} + \theta_f \rho_f \mathbf{g} + K_{gs}(\mathbf{u}_f - \mathbf{u}_s)$$

$$\boldsymbol{\tau} = \theta_s \mu_s (\nabla \mathbf{u}_s + (\nabla \mathbf{u}_s)^T) + \theta_s(\lambda_s - \frac{2}{3}\mu_s)(\nabla \cdot \mathbf{u}_s)\boldsymbol{\delta}$$

[1] J. Ding, D. Gidaspow, A Bubbling Fluidization Model Using Kinetic Theory of Granular flow, AIChE Journal vol. 36 No. 4 , 1990

Physical Models - DEM

Eulerian-Lagrangian Approach (Discrete Element Method, DEM) [2]

Multiphase CFD

Eulerian-lagrangian

DEM

Particle collision

$$F_{\text{contanct}} = F_{\text{normal}} + F_{\text{tangential}}$$

$$F_{\text{normal}} = k\delta + \lambda_0 v_n$$

δ = overlap
k= spring stiffness
v_n = relative velocity in normal direction
λ_0 = damping coefficient

$$F_{\text{tangential}} = -k_t \xi - \lambda_t v_t$$

ξ = overlap
k_t = tangential spring stiffness
v_t = relative velocity in tangential direction
λ_t = tangential dissipation parameter

$$\frac{\partial(\theta_f \rho_f)}{\partial t} + \nabla \cdot (\theta_f \rho_f \mathbf{u}_f) = \delta \dot{m}_{pf}$$

$$\frac{\partial(\theta_f \rho_f \mathbf{u}_f)}{\partial t} + \nabla \cdot (\theta_f \rho_f \mathbf{u}_f \mathbf{u}_f) = -\theta_f \nabla p + \theta_f \rho_f \mathbf{g} + \nabla \cdot (\theta_f \boldsymbol{\tau}_f) + \mathbf{F}$$

Solid phase

$$m_i \frac{d\mathbf{v}_i}{dt} = -V_i \nabla p + \frac{V_i \beta}{\theta_s}(\mathbf{u}_g - \mathbf{v}_i) + m_i g + F_{contact} \qquad I_i \frac{d\omega_i}{dt} = T_i$$

[2] S. Luding, Introduction to Discrete Element Methods, EJECE, pp 785, 2008

Physical Models - MPPIC

Eulerian-Lagrangian Approach (Multiphase Particle in Cell, MPPIC) [3]

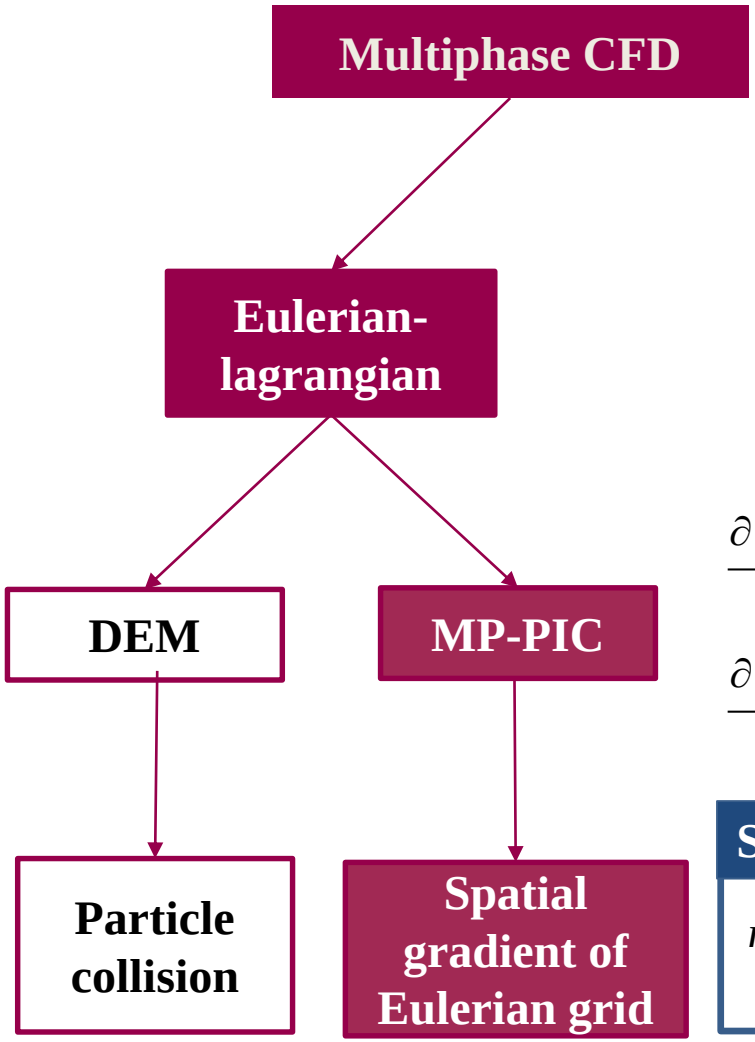

$$\tau_p = \frac{P_p \theta_p^{\beta}}{\max[(\theta_{CP} - \theta_p), \varepsilon(1-\theta_p)]}$$

θ_{CP} = closed pack volume fraction
ε = smallest number
P_p = particle pressure
β = constant ($2 \le \beta \le 5$)
τ_p = particle stress

$$F_{contact} = \frac{1}{\theta_p \rho_p} \nabla \tau_p$$

$$\frac{\partial(\theta_f \rho_f)}{\partial t} + \nabla \cdot (\theta_f \rho_f \mathbf{u}_f) = \delta \dot{m}_{pf}$$

$$\frac{\partial(\theta_f \rho_f \mathbf{u}_f)}{\partial t} + \nabla \cdot (\theta_f \rho_f \mathbf{u}_f \mathbf{u}_f) = -\theta_f \nabla p + \theta_f \rho_f \mathbf{g} + \nabla \cdot (\theta_f \boldsymbol{\tau}_f) + \mathbf{F}$$

Solid phase

$$m_i \frac{d\mathbf{v}_i}{dt} = -V_i \nabla p + \frac{V_i \beta}{\theta_s}(\mathbf{u}_g - \mathbf{v}_i) + m_i g + F_{contact}$$

[3] M.J. Andrews, R.J O'Rourke, The Multiphase Particle-in-Cell (MP-PIC) Method for Dense Particle Flows, International Journal of Multiphase Flow, 22(2):379–402. 1996

Physical Models

Particle Drag Model

- **Wen and Yu [4]**

$$F_{wen\&Yu} = \frac{\beta d_p^2}{\mu} = \frac{3}{4} C_D \,\mathrm{Re}\, \varepsilon_s \varepsilon_g^{-2.65} \quad C_D = \begin{cases} 24(1+0.15\,\mathrm{Re}^{0.687})/\mathrm{Re} & \text{if } \mathrm{Re} < 10^3 \\ 0.44 & \text{if } \mathrm{Re} > 10^3 \end{cases}$$

Appropriate for a dilute system

- **Ergun & Wen and Yu [5]**

1) $\varepsilon_s > 0.2$

$$F_{Ergun} = \frac{\beta d_p^2}{\mu} = 150 \frac{\varepsilon_s^2}{\varepsilon_g} + 1.75 \varepsilon_s \,\mathrm{Re}$$

2) $\varepsilon_s < 0.2$

$$F_{wen\&Yu} = \frac{\beta d_p^2}{\mu} = \frac{3}{4} C_D \,\mathrm{Re}\, \varepsilon_s \varepsilon_g^{-2.65}$$

Appropriate for a dense fluidized bed

[4] C. Y. Wen, Y. H. Yu, Mechanics of fluidization, Chemical Engineering Progress Symposium Series, vol.62,pp.100-111. 1966
[5] S. Benzarti, H. Mhiri, and H. Bournot, "Drag models for Simulation Gas-Solid Flow in the Bubbling Fluidized Bed of FCC Particles". World Academy of Science and Technology, Vol 6, 2012.01.21

Physical Models

Heat Transfer Model

$$m_i c_i \frac{dT_i}{dt} = hA_i(T_f - T_i) + \varepsilon A_i \sigma\left(\frac{G}{4\sigma} - T_i^4\right)$$

Convective heat transfer

Radiative heat transfer

$$Nu = \frac{hL}{k}$$

$$Nu = 2 + 0.6\,\mathrm{Re}^{0.5}\,\mathrm{Pr}^{1/3}$$

From Ranz & Marshall model

σ : Stefan-Boltzan constant

G : incident radiation

c_i : specific heat

A_i : surface area

ε : emissivity

Discrete Particle Model (DPM)

$$F_{in} = n\,F_{i1} \qquad de_n = n\,de_1$$

$$dm_n = n\,dm_1$$

n : particles per parcel

de : heat transfer

dm : mass transfer

Physical Models

Surface Reaction – Random Pore Model

- Coal gasification slower than reduction of iron oxide so that the overall reduction rate is controlled by carbon gasification reaction at temperatures below 1100ºC [6,7].

- Carbon gasification rate estimated by the Random Pore Model [8].

$$\frac{dx}{dt} = k_p(1-x)\sqrt{1-\psi\ln(1-x)}$$

$$\frac{S}{S_0} = (1-x)\sqrt{1-\psi\ln(1-x)}$$

$$\psi = 4\pi L_0(1-\varepsilon_0)/S_0^{\,2}$$

ψ : *initial pore structure,*

L_0 : *initial pore length,*

ε_0 : *initial porosity,*

S_0 : *initial specific surface area*

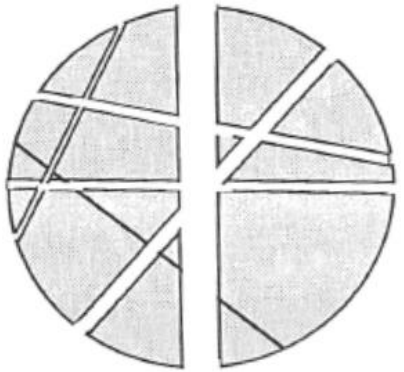

GAVALAS
(random pore model)

[6] R. Fruehan, The rate of reduction of iron oxides by carbon, Metallurgical Transactions B 8 (1) (1977) 279-286

[7] D. Santos, M. Mourao, High-temperature reduction of iron oxides by solid carbon or carbon dissolved in liquid iron–carbon alloy, Scandinavian Journal of Metallurgy 33 (4) (2004) 229-235

[8] S.K Bhatia, D.D, Perlmutter, A random pore model for fluid-solid reactions: I. Isothermal, Kinetic Control, AIChE vol.26 No.3 Pp379-385, 1980

Turbulent Combustion Model

▪ Eddy Dissipation Model (EDM)

- The net rate of production of species *i* due to reaction *r*, $R_{i,r}$, is given by the smaller (i.e., limiting value) of the two expressions below:

$$R_{i,r} = v'_{i,r} M_{w,i} A \rho \frac{\varepsilon}{k} \min_R \left(\frac{Y_R}{v'_{R,r} M_{w,R}} \right) \qquad R_{i,r} = v'_{i,r} M_{w,i} A B \rho \frac{\varepsilon}{k} \frac{\sum_P Y_P}{\sum_j^N v''_{j,r} M_{w,j}}$$

where

Y_P = the mass fraction of any product species, *P*

Y_R = the mass fraction of a particular reactant, *R*

A = an empirical constant equal to 4.0

B = an empirical constant equal to 0.5

- The mean reaction rate is governed by the large-eddy mixing time scale, k/ε.

- Multi-step chemical mechanism is based on the Arrhenius rates, which differ for each reaction. In the EDM every reaction has the same turbulence scale, therefore EDM should be used only for one-step or two-step global reactions.

Code Development - MPPIC

Code Development for Fluidized Beds (OpenFOAM ver 2.3.x)

MPPIC library

- MPPIC particle motions
- Incompressible turbulence model

+

Turbulence model library

- **Modified the standard k-e model for volume fraction of particles**

+

Diffusion method library

- **Adhoc diffusion for convergence**

ReactingParcelFoam Solver

- Surface reactions of particles can be analyzed
- Gas Phase reaction can be analyzed
- Compressible Turbulence model
- **EDM was applied**
- **Volume fraction**

Final solver for a fluidized bed

- MPPIC motion and surface reaction of particles
- Compressible Turbulence Model
- Apply the diffusion method to reduce # of particles

Code Development - DPM

Code Development for Rotary Kilns (OpenFOAM ver 2.3.x)

Final solver for fluidized bed

- MPPIC motion and surface reaction of particles
- Compressible Turbulence Model
- Apply the diffusion method to reduce # of particles

+

DPM library

- **DPM motion of particles can be analyzed**
- **Incompressible Turbulence Model**

+

Coal Combustion

- **Devolatilization Model**
- **Char Combustion Model**

Final solver for a rotary kiln

- DPM motion and surface reaction of particles
- Compressible Turbulence Model
- Apply the diffusion method to reduce # of particles
- Coal combustion can be analyzed

Code Development – Diffusion Method

Reduce the Number of Computational Parcels

- Reducing the parcels in MPPIC increased computational instability. The diffusion method may suppress such instability to some extent.

- Statistical kernel method

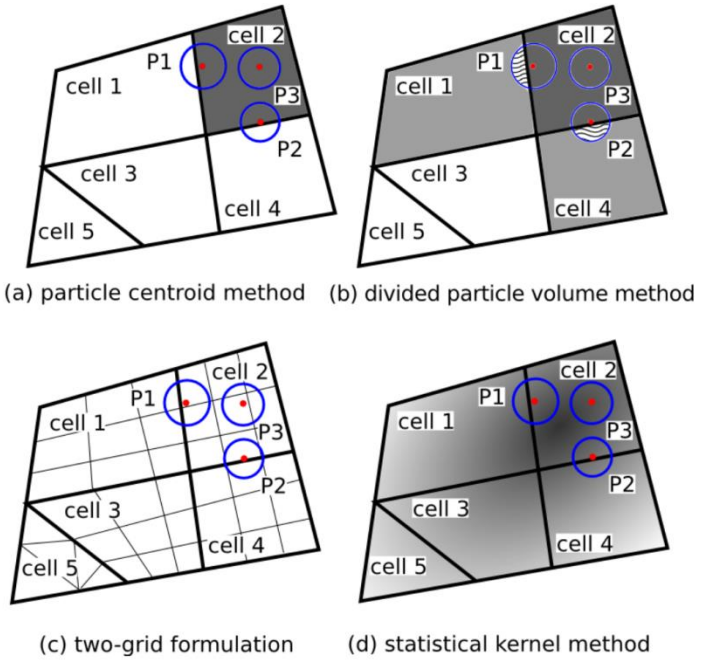

(a) particle centroid method (b) divided particle volume method

(c) two-grid formulation (d) statistical kernel method

$$\frac{\partial \varepsilon}{\partial \tau} = \nabla^2 \varepsilon \quad \text{for} \quad \mathbf{x} \in \mathbb{R}^3, \tau > 0$$

$$\varepsilon(\mathbf{x}, 0) = \varepsilon_0(\mathbf{x})$$

$$G(\mathbf{x}, \tau) = \frac{1}{(4\pi\tau)^{3/2}} \exp\left[-\frac{\mathbf{x}^T \mathbf{x}}{4\tau}\right]$$

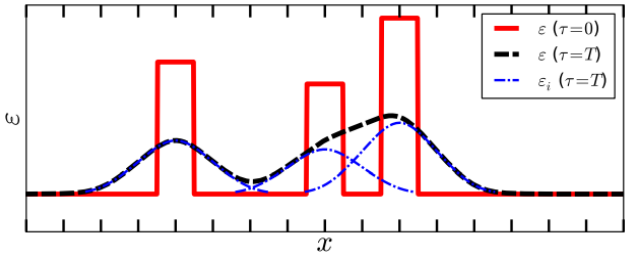

Diffusion method [9]

[9] Rui Sun, H. Xiao, Diffusion-based coarse graining in hybrid continuum-discrete solvers : Applications in CFD-DEM 2015, International journal of multiphase flow, vol 72, pp 233-247

Code Validation

Validation Case

- **Muller Case setup[10]**

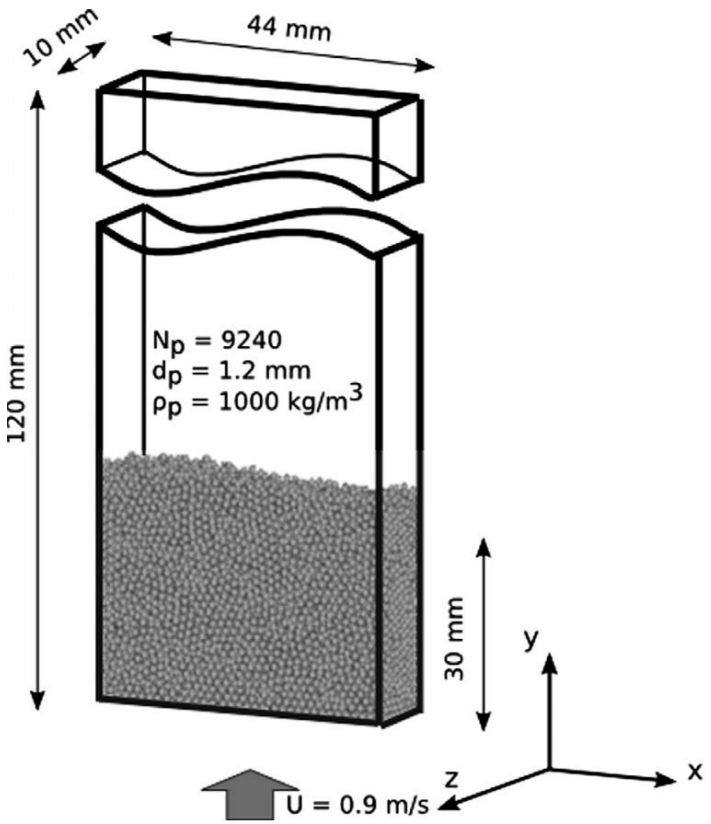

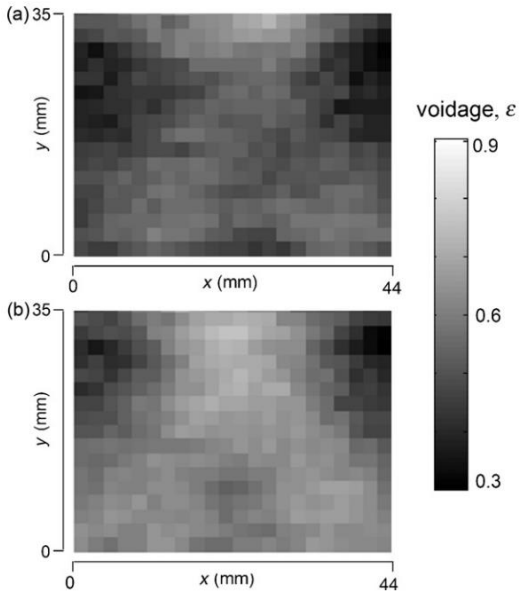

MR measurements of the time-averaged voidage

Operating Conditions	
Inlet velocity (m/s)	**0.9 / 0.6**
Inlet Gas	**Air**
Gas density (kg/m^3)	**1.2**
Particle diameter (mm)	**1.2**
Particle density (kg/m^3)	**1000**
Parcel number	**9240**
Operating time (sec)	**23**

[10]C. R.Muller, S.A. Scott, D.J. Holland, B.C Clarke, Validation of a discrete element model using magnetic resonance measurements, 2009, Particulogy, vol 7, pp 297 – 306

Code Validation

Validation Results

- The diffusion method was applied for the 100 parcels case.
- Calculation diverged without the diffusion method.

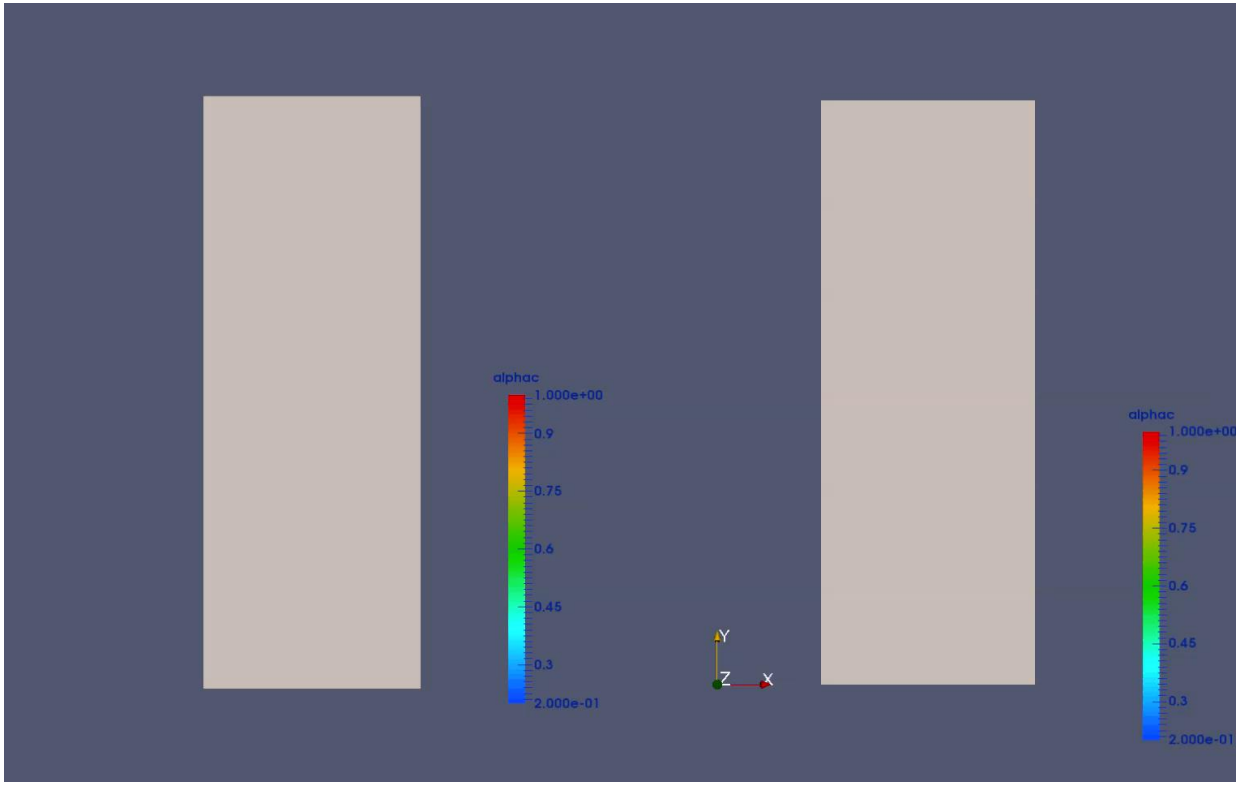

Parcel 9000(No Diffusion)

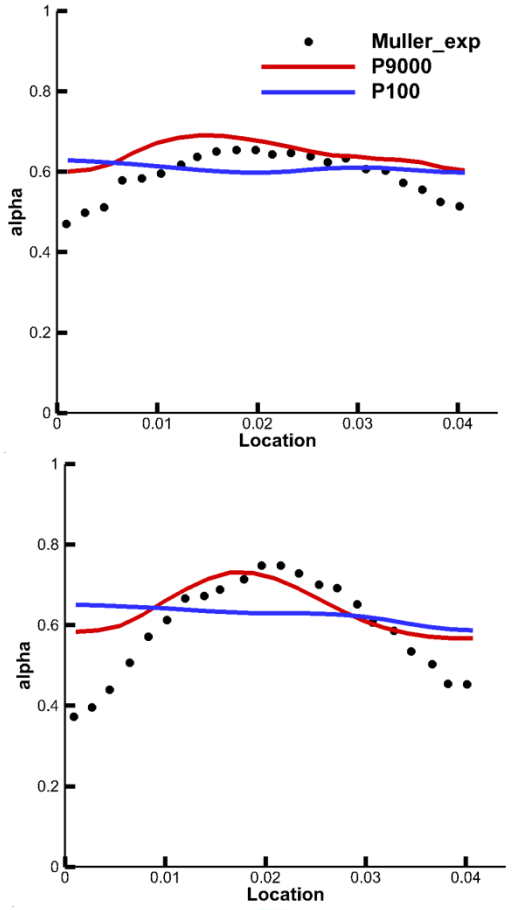

Parcel 100 (Diffusion)

Application - Fluidized Bed

Fluidized Bed for the Steel Making Process (FINEX)

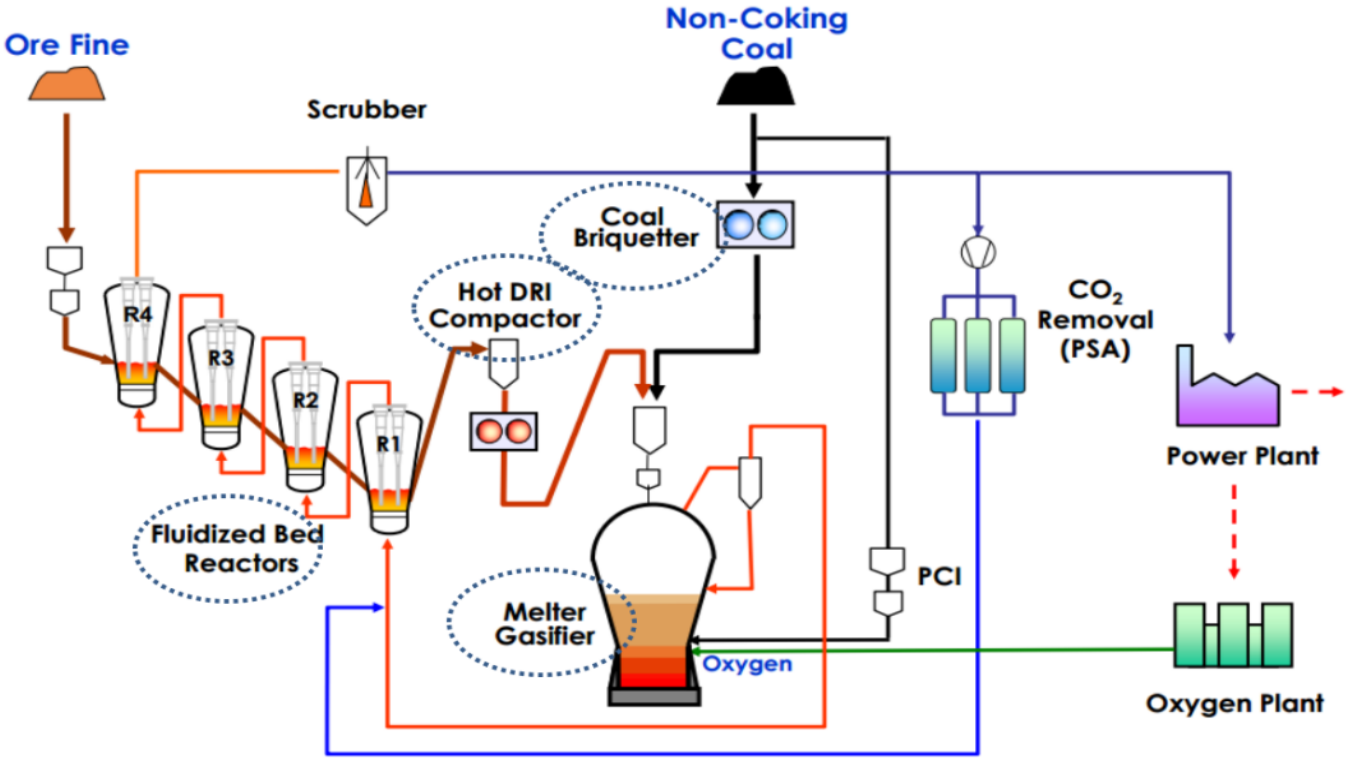

- Particular iron ore reduced in fluidized beds in the FINEX process.
- Reduced iron and bituminous coal reproduced as HCI(Hot Compacted Iron) and briquette coal, which are mixed in the melter-gasifier to produce liquid iron.

Application - Fluidized Bed

Geometry and Operating Conditions

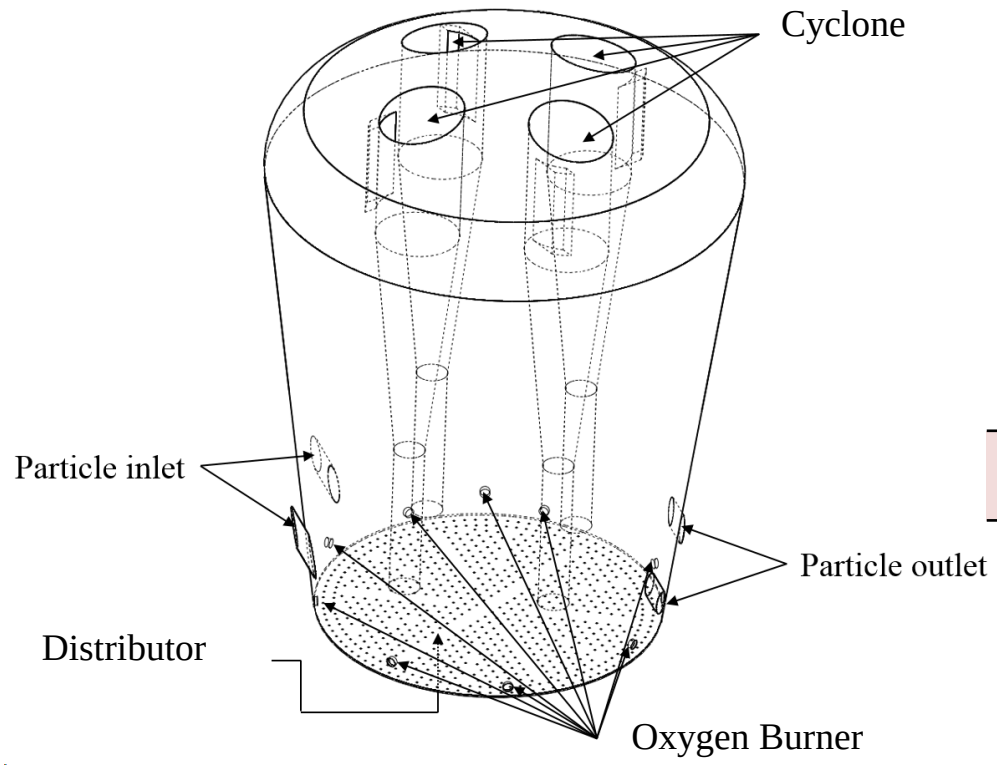

Conditions	Combustion
OpenFOAM 2.3x	EDM (Eddy Dissipation Model)
4.5 million structured cell	1. $CH_4 + 1.5O_2$-> $CO + 2H_2O$
Pressure outlet (4.5bar)	2. $CO + 0.5O_2$ -> CO_2
Cyclic boundary condition	3. $H_2 + O_2$ -> H_2O
Standard k-e turbulence model	

Distributor gas fraction	(mole fraction)	Burner gas fraction	ratio
H_2	15.3	N_2 / O_2	2 / 1
H_2O	6.1	Distributor Jet Vel	119.28 m/s
CO	43.2	Distributor Jet Temp	1083K
CO_2	21	Burner Jet Vel	120 m/s
CH_4	1.6	Burner Jet Temp	298K
N_2	12.8		

Application - Fluidized Bed

Flame Shape of a Bed Burner

- Jets from the distributor and the oxygen burner show interaction with each other.
- The flame tends to spread due to such interaction.

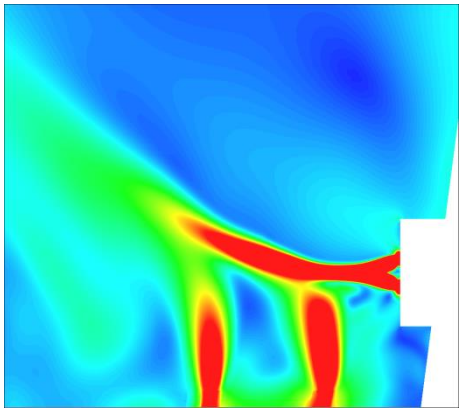

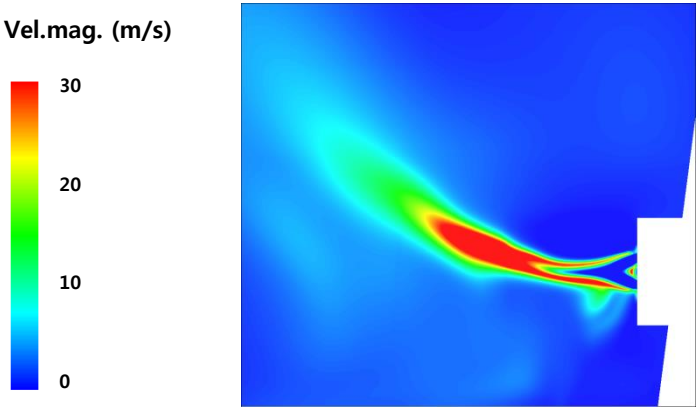

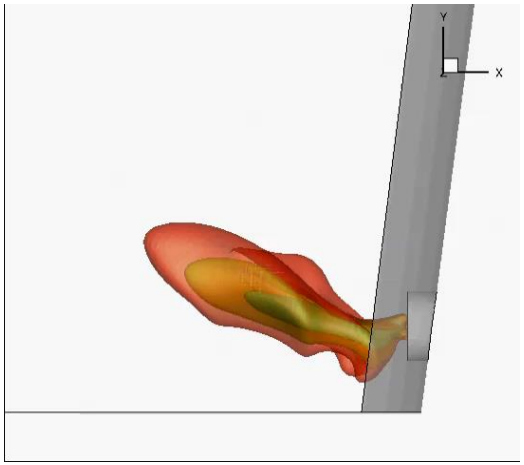

Iso temperature surface (X-axis rotation)

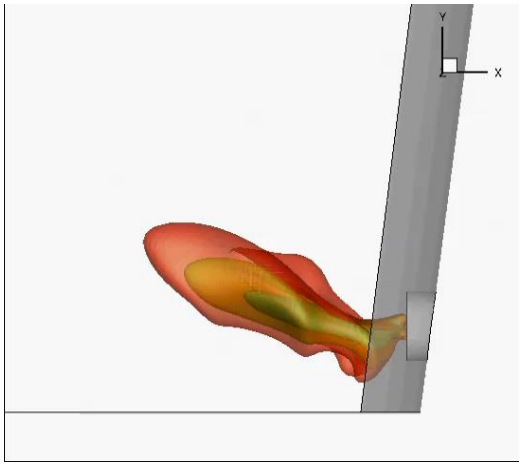

Iso temperature surface (Y-axis rotation)

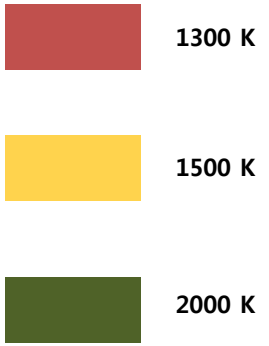

Application - Fluidized Bed

Internal Fields

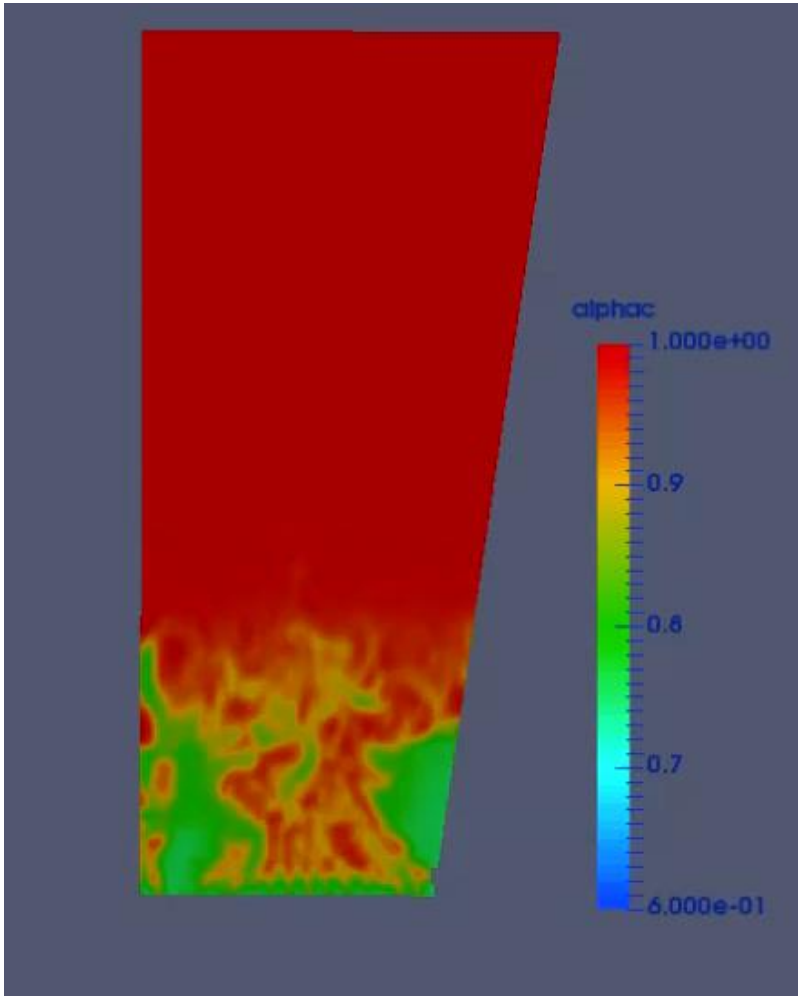

Gas volume fraction

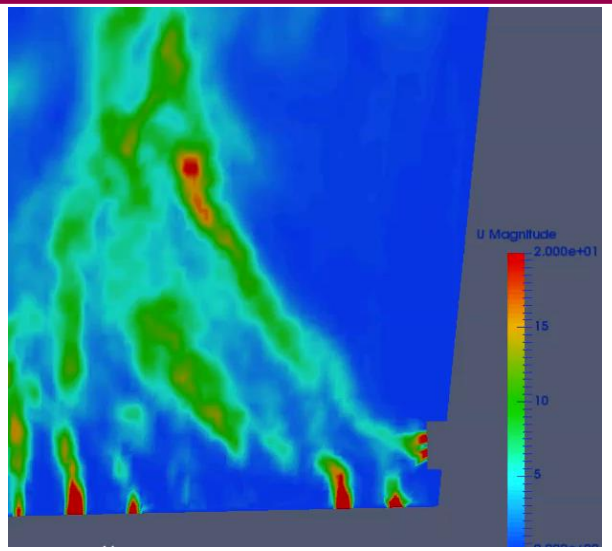

Velocity

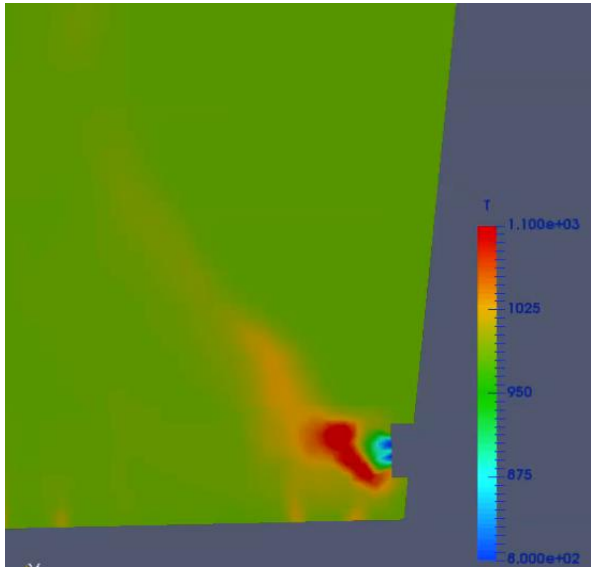

Temperature

Application - Fluidized Bed

Particles Motion and Temperature Variation

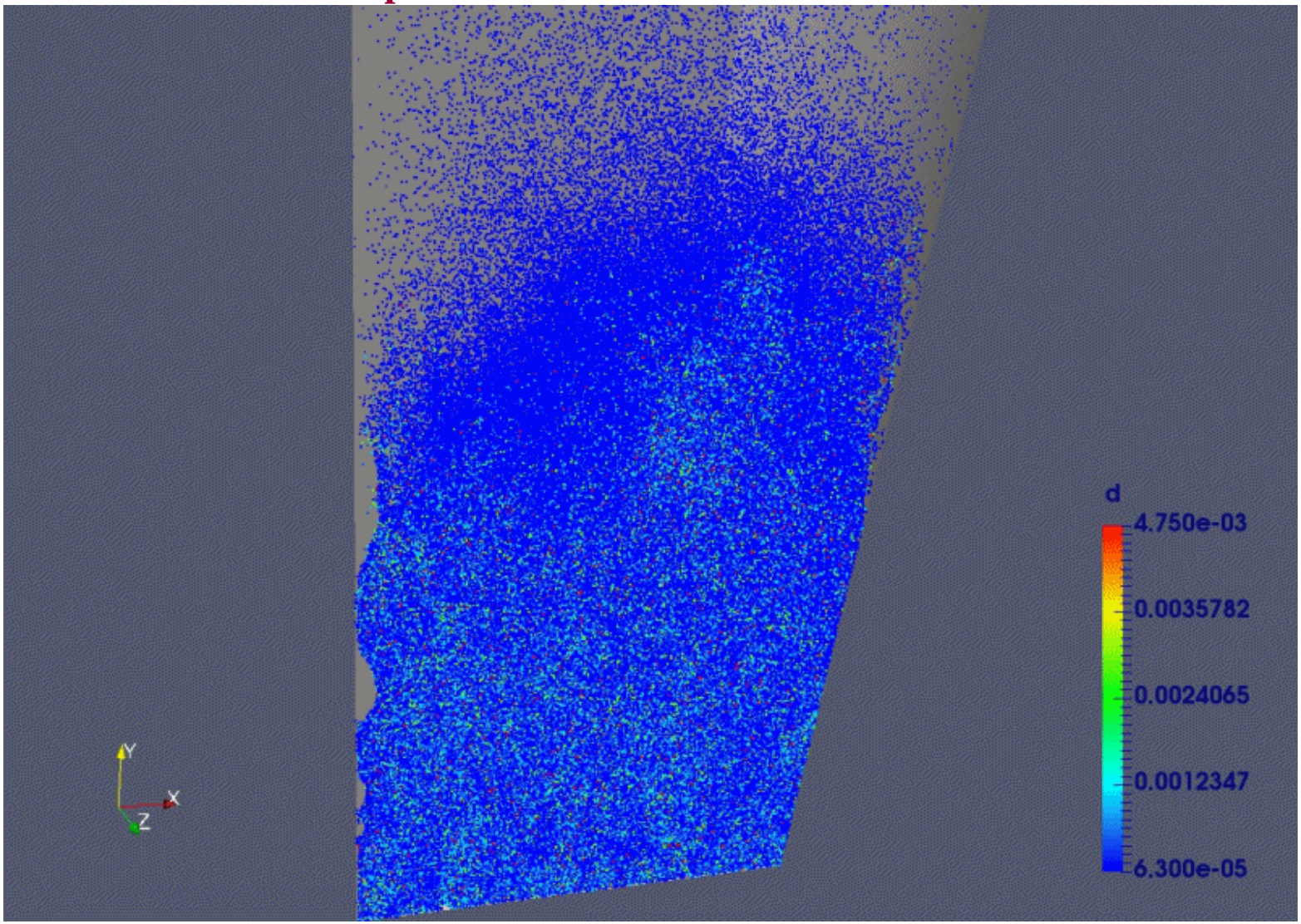

Application - Fluidized Bed

Particles Motion and Temperature Variation

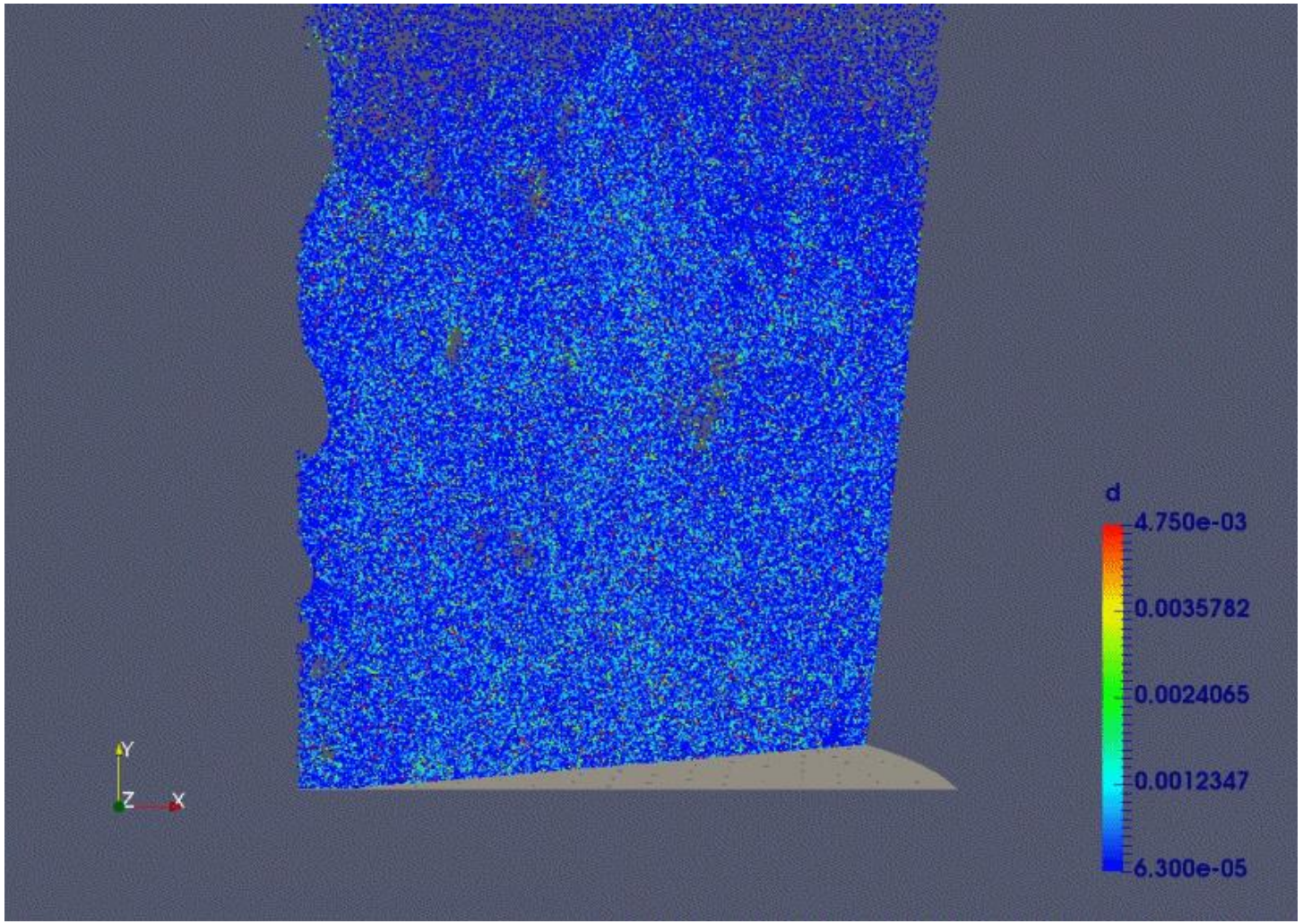

Near the distributor nozzles

Application - Fluidized Bed

Results

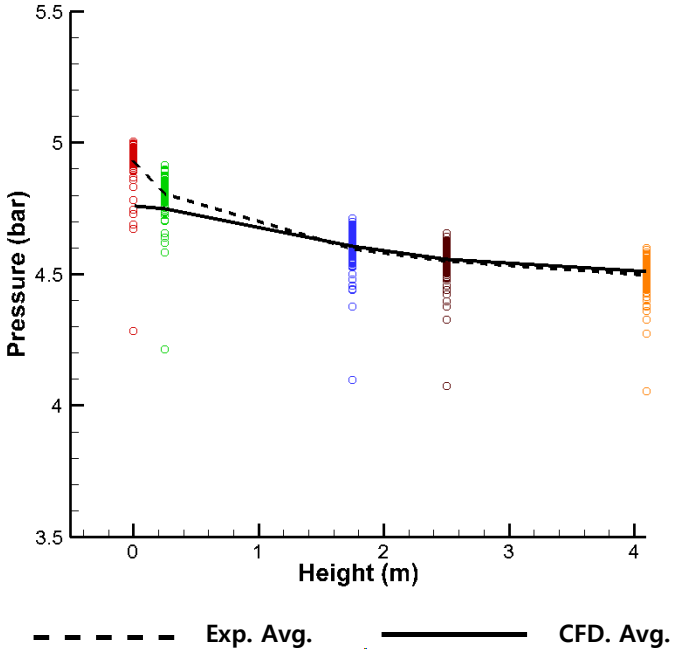

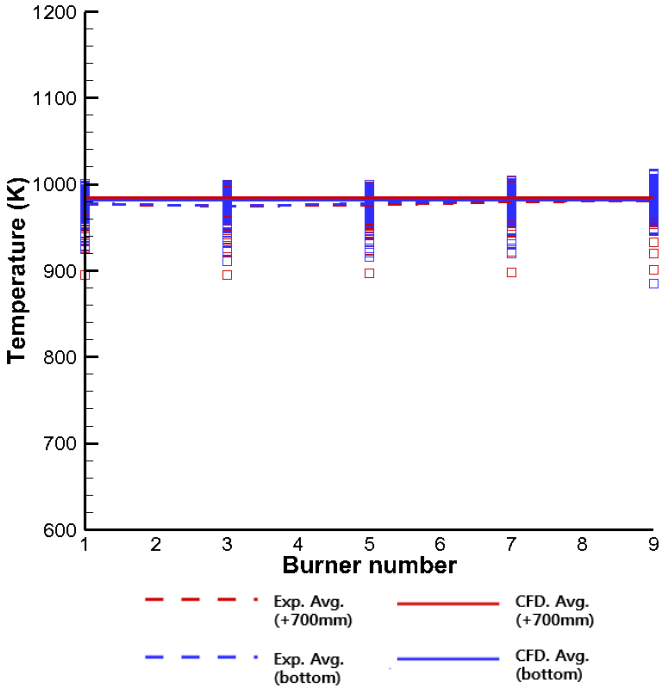

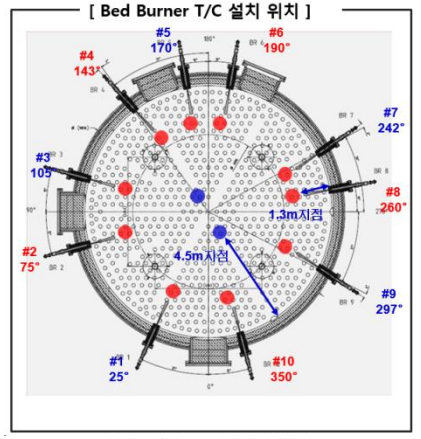

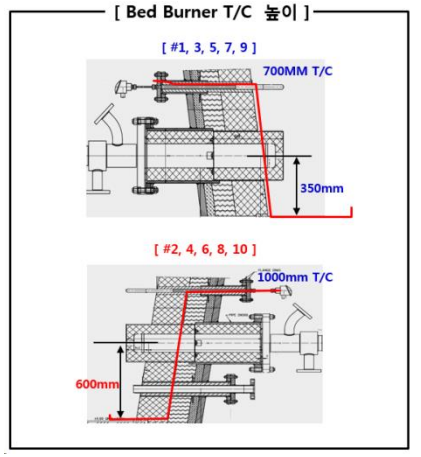

Application – Moving Bed

Rotary Kiln

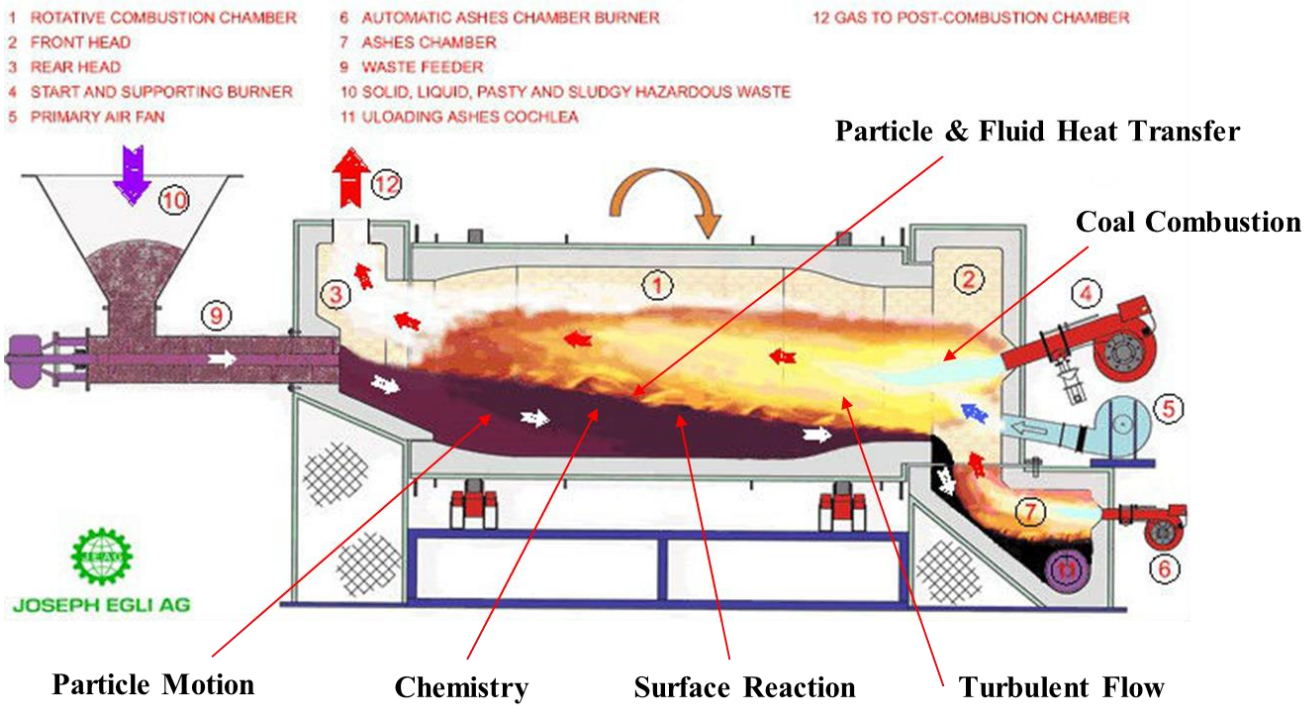

- Pre-reduction for uniform particles and dehydration before entering the electric arc furnace.
- Continuous flow reactor - Rotating wall driving radial particle motion, while the tilted wall driving axial particle motion.

Application - Moving Bed

Rotary Kiln – Transverse Motion [11]

- Bed particle motion in slumping, transition, rolling and slipping modes.
- The effects of rotational speed, bed depth, cylinder diameter and particle size were taken into account.

Experimental Conditions

Property	Range
Material	Limestone
Kiln axial length (m)	0.46
Kiln diameter (m)	0.4
RPM range (rpm)	0.5 ~ 10
Bed depth range (m)	0.03 ~ 0.07
Particle diameter (mm)	4.3
Angle of Slip(Degrees)	43.9

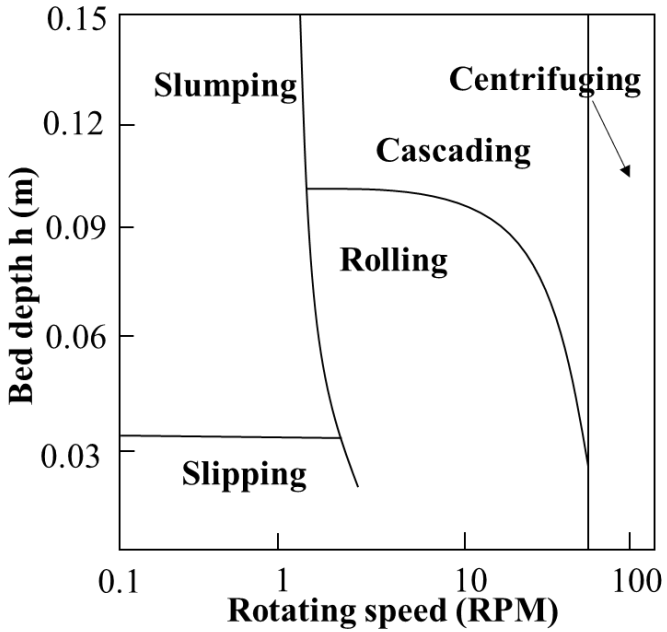

Regime Map[12]

[11] H. Henein , J.K. Brimacombe, A.P. Watkinson, Experimental Study of Transverse Bed Motion in Rotary Kiln, Metallurgical Transactions B, pp191-205, 1983
[12] H. Henein , J.K. Brimacombe, A.P. Watkinson, The Modeling of Transverse Solids Motion in Rotary Kilns, Metallurgical Transactions B, pp207-220, 1984

Application - Moving Bed

Rotary Kiln – Transverse Motion

- Rotating speed =10rpm

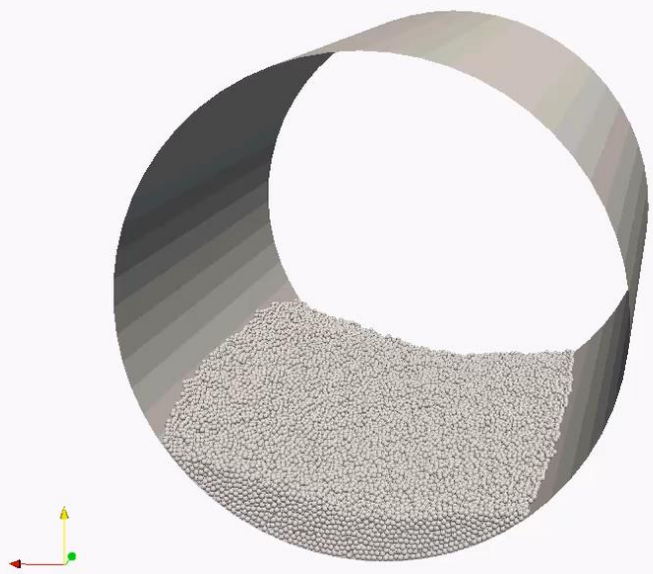

Bed depth = 0.053m

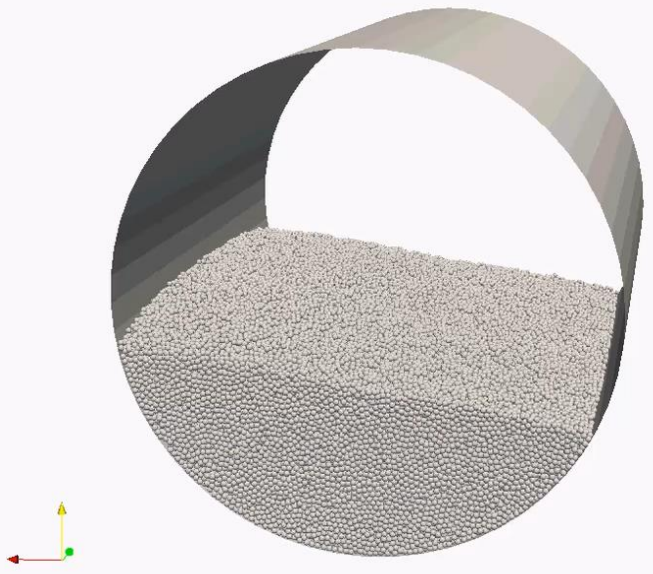

Bed depth = 0.15m

- The external bed shape remains stationary as particles slide down the top surface forming an active layer and an inactive region in the interior. – Rolling Mode

Application - Moving Bed

Rotary Kiln – Transverse Motion

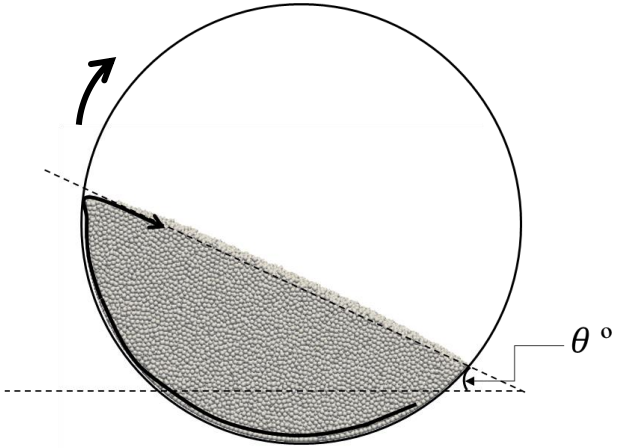

Particles in the rolling mode

Case #	rpm	h (m)	θ(º)	Mode
1	10	0.053	25.6	Rolling
2	10	0.07	24.3	Rolling
3	10	0.15	24.0	Rolling
4	30	0.053	22.9	Rolling
5	30	0.07	23.0	Rolling
6	30	0.15	25.2	Rolling

- The particles were in the rolling mode s at 10 rpm with the inclination angle, θ between 24º ~ 25.6º.
- The inclination angle decreased as the bed depth increasing.
- Case 3, 6 were predicted cascading motions in Henein's paper. However the simulation shows both cases are in rolling motion.

Application - Moving Bed

Rotary Kiln – Transverse Motion

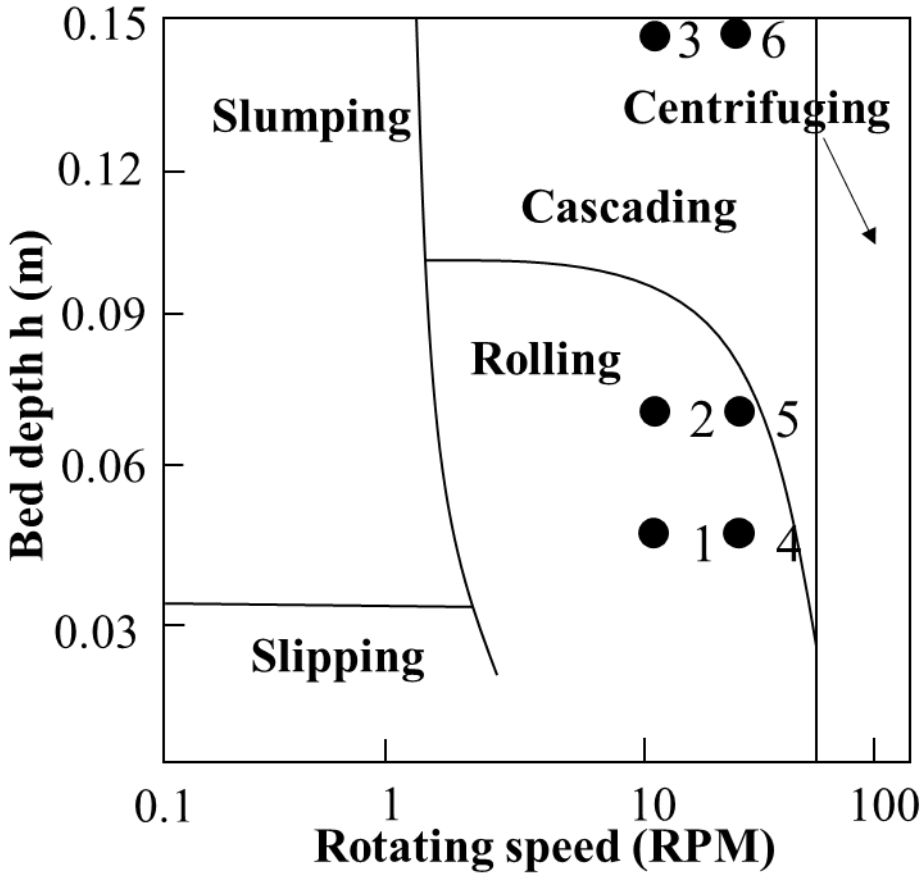

Transverse particle motion in the regime map

Application - Moving Bed

Rotary Kiln – Reduction [13]

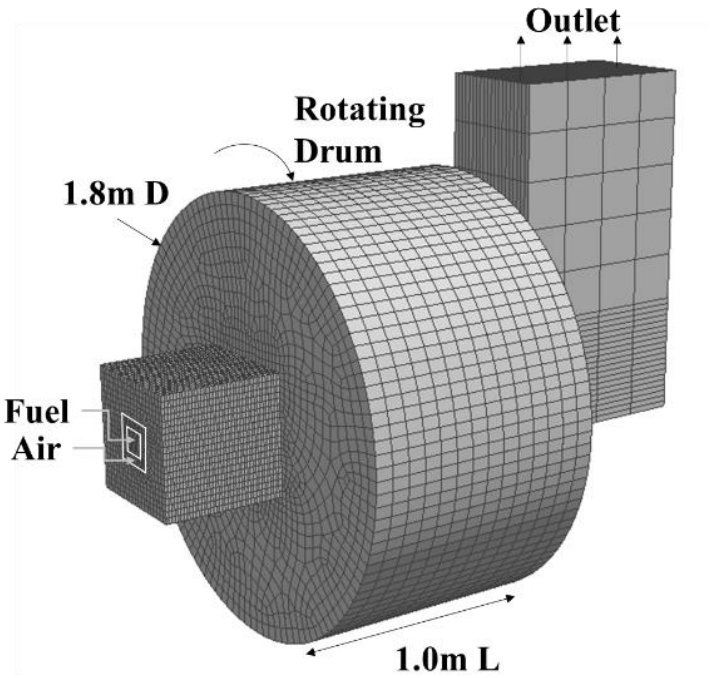

Computational mesh for the pilot scale rotary kiln

Experimental Conditions

Property	Value
RPM	0.33
Ore (kg)	560
Coal(Anthracite) (kg)	101
Limestone (kg)	44.0
Particle size (mm)	30x25x15
Fuel	LPG
Fuel mass flow rate(m^3/h)	30
Air mass flow rate(m^3/h)	709.5

Ore compositions in Tsuji

Chemical	Mass%
SiO_2	44.36
Fe	9.05
Al_2O_3	0.41
Ni	2.45
CaO	0.08
MgO	26.68

[13] H. Tsuji, Behavior of Reduction and Growth of Metal in Smelting of Saprolite Ni-ore in a Rotary Kiln for Production of Ferro-nickel Alloy, 2011

Application - Moving Bed

Rotary Kiln – Temperature and Reduction Chemistry

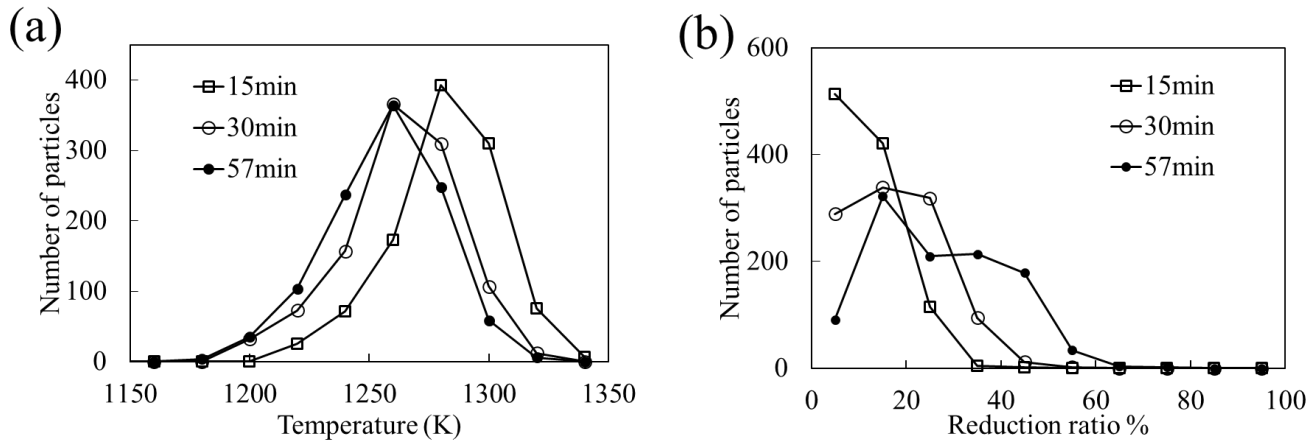

Probability distributions of particle temperatures (a) and reduction ratios (b) in the pilot scale rotary kiln

- Particle temperatures decreased initially to reach the quasi-equilibrium state, closely following the normal distribution peaking at 1260K after about 30 minutes.
- The mean reduction ratio increased monotonously, showing wider distribution of the reduction ratio with the calcination time.

Application - Moving Bed

Rotary Kiln – Temperature and Reduction Chemistry

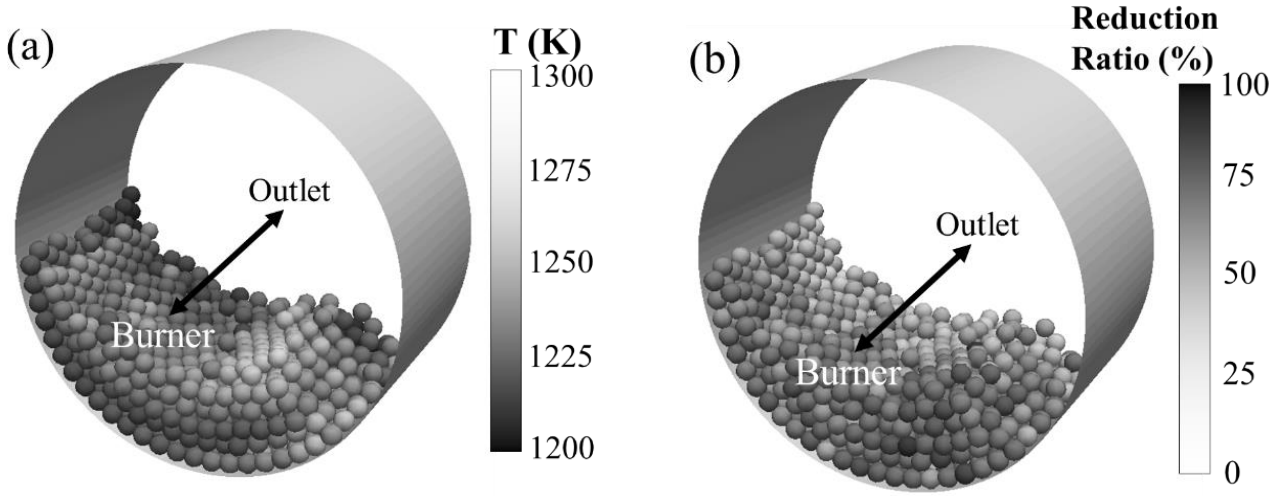

Temperature (a) and reduction ratio (b) of particles at 57minutes in the pilot scale rotary kiln

- Particles showed higher temperatures and higher reduction ratios near the burner due to higher heat transfer rate from freeboard gas at its maximum temperature.
- The reduction ratio was relatively uniform due to efficient mixing in the radial direction while particles showed higher temperatures on the bed surface due to heat transfer from freeboard gas.
- Heat transfer occurs faster than particle mixing and reduction chemistry to maintain nonnegligible temperature gradient in the bed.
- Inefficient mixing in the axial direction as compared with mixing of particles in the radial direction.

Application - Moving Bed

Rotary Kiln – Temperature and Reduction Chemistry

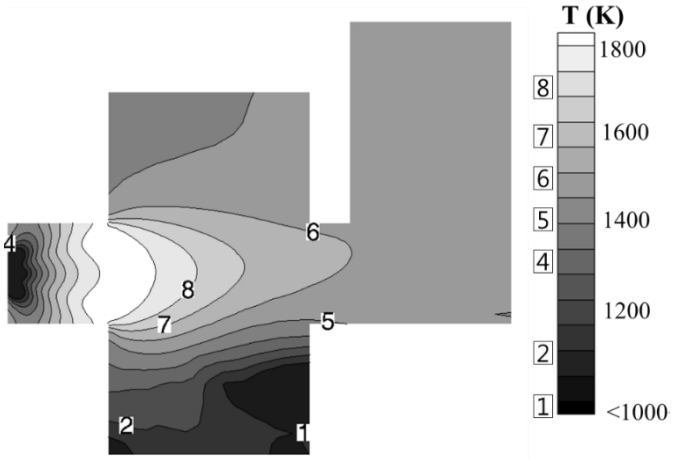

Temperature distribution in the pilot scale rotary kiln

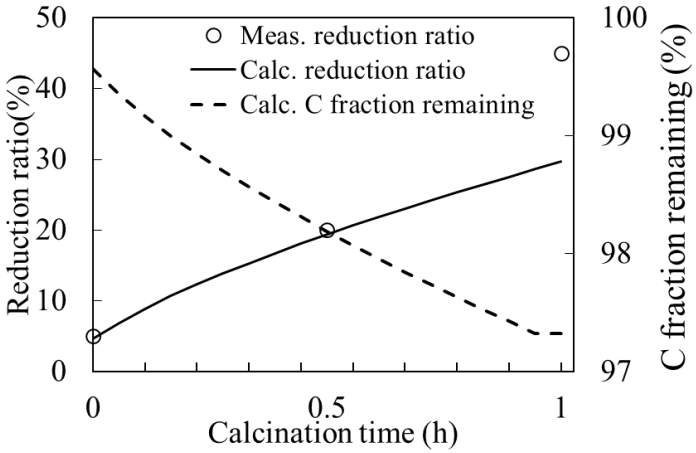

Calculated reduction ratio and carbon fraction remaining with respect to calcination time

- Note lower temperatures in the bed due to the heat sink by endothermic coal gasification reaction.
- Heat release by combustion about 805 kJ/sec. Sensible enthalpy leaving the outlet about 329 kJ/sec. The difference of 476 kJ/sec corresponds to the energy consumed by reduction chemistry with adiabatic wall boundaries.
- Solid carbon in coal is consumed with the carbon fraction decreasing continuously to produce carbon monoxide by heterogeneous reaction.

Summary

- The libraries were developed for combustion and particle motion in OpenFOAM and applied for two engineering problems of a fluidized bed and a moving bed.
- The diffusion method was applied successfully for convergence with a reduced number of computational parcels in MPPIC.
- The MPPIC method was applied to a fluidized bed reactor in the FINEX process. Results showed reasonable trends for particle motion and bed burners in the R2 reactor.
- The DPM was validated for slumping and rolling modes of particle motion in the regime map of a rotary kiln by Henein et al.
- The DPM was applied to a laboratory kiln. Variation of particle temperatures and reduction ratios in the radial as well as in the axial direction in the bed. Gasification and reduction continued with the calcination time, while particles reached the quasi-equilibrium temperature distribution according to overall energy balance.

Thank you